

## A generic 1-D imaging method for transient electromagnetic data

Niels Bøie Christensen\*

### ABSTRACT

This paper presents a fast approximate 1-D inversion algorithm for transient electromagnetic (EM) data that can be applied for all measuring configurations and transmitter waveforms and for all field components. The inversion is based on an approximate forward mapping in the adaptive Born approximation. The generality is obtained through a separation of the forward problem into a configuration-independent part, mapping layer conductivities into apparent conductivity, and a configuration-dependent part, the half-space step response. The EM response from any waveform can then be found by a convolution with the time derivative of the waveform. The approach does not involve inherently unstable deconvolution computations or nonunique transformations, and it is about 100 times faster than ordinary nonlinear inversion. Nonlinear model responses of the models obtained through the approximate inversion fit the data typically within 5%.

### INTRODUCTION

In Denmark, transient electromagnetic (EM) soundings have become one of the standard methods of environmental geophysics, especially for large-scale hydrogeological investigations (Fittermann and Stewart, 1986; Buselli et al., 1990; Hoekstra and Blohm, 1990; Christensen and Sørensen, 1998). Transient measurements can delineate good conductors such as clay and salt water, which constitute the effective lower boundaries of freshwater resources over most of the Jutland peninsula. The strategy has been to obtain transient soundings over the target area at a density of 16 to 25 soundings per km<sup>2</sup>.

The success of transient soundings in hydrogeological investigations has led to the development of pulled-array transient electromagnetic equipment (PATEM), where a transmitter loop and a receiver coil are towed over the ground while continuously measuring data (Sørensen, 1997; Sørensen et al., 1995, 2000). The density of transient soundings with the PATEM system is approximately 20 m on the profile lines, pro-

ducing more than 5000 soundings a day. Compared with airborne measurements, the PATEM data set has more early time information and thereby a better resolution of near-surface conductivity.

During the last two decades large-volume data sets have been collected with airborne transient EM systems (Macnae et al., 1991). The density of measurements on the survey lines is typically on the order of 10 m, often resulting in data volumes of millions of soundings. Airborne measurements also find increased use in hydrogeophysical mapping.

Traditionally, single-site transient soundings have been interpreted with 1-D earth models; with the speed of modern computers, this type of interpretation is no longer a computational problem. However, it is now possible to collect large data sets of good quality warranting a quantitative interpretation, so the need for fast interpretation procedures persists. Data from airborne surveys and profile-oriented, continuous, ground-based systems like PATEM are time consuming to interpret with full nonlinear methods. An imaging algorithm for fast approximate interpretation is desirable to provide a quick overview of results. The models resulting from an approximate interpretation provide good starting models for full nonlinear inversion and thereby speed up the interpretation process (Stolz and Macnae, 1997). The computer-based design of modern transient instruments makes it important to develop fast, in-field interpretation techniques that can help field crews assess data quality and determine the location of future measurements.

The term imaging has been used in many different contexts in geophysics, indicating in a general sense the interpretation of geophysical data. In this paper the term is used to mean an approximate inverse mapping of data into a model.

Most EM imaging methods presented in the literature are based on knowing the step-response. Pure step-response data are almost impossible to obtain, so a deconvolution of the measured data to find the step response is necessary. This is an inherently unstable problem. Some methods also require an all-time apparent conductivity to be determined from the step response—a problem that is often nonunique.

In the process of diffusion of transient EM fields into the ground, the diffusion depth and diffusion velocity depend on the subsurface conductivity structure. A number of imaging

Manuscript received by the Editor June 28, 2000; revised manuscript received July 12, 2001.

\*University of Aarhus, Department of Earth Sciences, Finlandsgade 8, DK-8200 Aarhus N, Denmark. E-mail: nbc@geo.au.dk.  
© 2002 Society of Exploration Geophysicists. All rights reserved.

methods are based on the variation of the diffusion velocity with conductivity (Nekut, 1987; Macnae and Lamontagne, 1987; Eaton and Hohmann, 1989; Macnae et al., 1991). These algorithms find the depth to an equivalent current filament—an image of the source—as a function of time, from which the diffusion velocity and thereby the conductivity can be found. The conductivity is then ascribed to a depth equal to the image depth scaled with an ad hoc factor to produce the best results. Macnae and Lamontagne (1987) use a number of such images instead of just one. Christensen (1995) presents an imaging method based on the all-time apparent conductivity of the step response, a method extended to the 2-D case in Christensen (1997). The conductivity-depth imaging of Stolz and Macnae (1997) is based on the step response, and Stolz and Macnae (1998) present a method for reducing arbitrary waveform transient EM data to the step response.

Smith et al. (1994) develop an imaging algorithm for coincident loop soundings using the Fréchet kernel and the impulse-response apparent resistivity. The apparent resistivity is ascribed to the depth of the Fréchet kernel maximum. However, the use of the impulse-response apparent resistivity instead of that for the step response gives erratic results with overshoots and undershoots. [For a thorough discussion of apparent resistivity, see Spies and Eggers (1986).]

Polzer (1985) considers time as a function of the magnetic field and develops a theory for inversion of arrival time data of a certain amplitude of a magnetic field. Using a linear approximation to the Fréchet kernel, he develops a one-step imaging inverse where the diffusion depth is scaled according to the arrival time of a reference model, a homogeneous half-space. This scaling of the arrival-time Fréchet kernel is completely equivalent to the one-pass imaging algorithm of Christensen (1995), with scaling according to all-time apparent conductivity.

In this paper a new approach to 1-D imaging of transient data is presented. The method is based on an approximate forward mapping of a layered conductivity structure to apparent conductivity and does not require deconvolution or any nonunique transformations. The approximate representation can then be inverted to yield an estimate of the subsurface conductivity structure. Furthermore, the method possesses a high degree of generality and can be used for any EM system and an arbitrary current waveform.

### SEPARATION OF THE FORWARD PROBLEM

The imaging procedure defined in the following sections is based on the construction of an approximate forward mapping and ordinary inversion theory for a nonlinear inversion problem. The construction of the forward mapping is based on the following observed steps.

First, the response measured in an induction coil from any current waveform used in a transient EM transmitter can be expressed as a function of the step response. This relies on the fact that the response of an induction coil is the convolution between the impulse response and the time derivative of the waveform. The calculation is often done by approximating the waveform with a piecewise linear and continuous function, in which case the measured response is expressed as a linear combination of values of the step response.

Second, the observed step response is by definition the EM response for a half-space having a conductivity equal

to the apparent conductivity  $\sigma_a(t)$ , based on the step response  $H^{step}(t) = H_{half-space}^{step}(t, \sigma_a(t))$ . The EM response depends, of course, on geometrical configuration, transmitter-current waveform, and system bandwidth. For configurations for which the step response apparent conductivity can be defined, it is often called the all-time apparent conductivity (Spies and Eggers, 1986).

Third, if we can find a suitable approximation to the all-time apparent conductivity, i.e., formulate a mapping from model conductivities  $\sigma_i(z)$  to apparent conductivity  $\sigma_a(t)$ , we avoid unstable operations such as deconvolutions and nonunique transformations. This is general forward mapping from model conductivity to apparent conductivity. Substituting the apparent conductivity into the configuration-dependent half-space response in observation 2 is a simple, uniquely defined, stable forward calculation for all measurement configurations. Observation 1 is a simple linear combination of values of the step responses. Steps 2 and 3 can be illustrated by

$$H^{step}(t) = H_{half-space}^{step}[t, \sigma_a(t, \sigma(z))]. \quad (1)$$

### GENERIC APPROXIMATE FORWARD MAPPING

Following the ideas of the previous section, I suggest the following generic forward mapping of a 1-D conductivity structure  $\sigma(z)$  where the conductivity is only a function of depth  $z$  into an apparent conductivity  $\sigma_a(t)$  as a function of time  $t$ :

$$\sigma_a(t) = \int_0^\infty \sigma(z) \cdot f(z, t, \sigma_a(t)) dz, \quad (2)$$

where the sensitivity function  $f$  is approximated by

$$f(z, t, \sigma_a(t)) = \begin{cases} \frac{2}{d} \left(1 - \frac{z}{d}\right) & \text{for } z \leq d \\ 0 & \text{for } z > d \end{cases}, \quad (3)$$

where

$$d = \sqrt{\frac{ct}{\mu_0 \sigma_a(t)}}.$$

The ad hoc scaling factor  $c$  is to be determined later through an optimization procedure, and  $\mu_0$  is the magnetic permeability of free space.

Equation (2) is an approximation and a nonlinear integral equation (Gomez-Treviño, 1987). Choosing  $\sigma_a(t)$  to be a constant, the formulation would become a Born approximation, with  $f$  being the Fréchet derivative. In this case equation (3) defines an approximation to  $f$  that decreases linearly from the surface down to the scaled diffusion depth  $d$  and is zero below this depth. Figure 1a shows the sensitivity function as a function of depth for a half-space resistivity of 10 ohm-m and delay times 10, 50, and 200  $\mu$ s.

Using the actual apparent conductivity  $\sigma_a(t)$  instead of a constant conductivity in equations (2) and (3) has the effect that the slow diffusion of transient EM fields through good conductors and the fast diffusion through poor conductors is reflected in the value of the scaled diffusion depth. In this way the forward mapping becomes sensitive to the distribution of conductivity in the subsurface, a property previously termed adaptive Born approximation (Christensen, 1995, 1997). I therefore call the mapping described here ABFM (Adaptive Born Forward Mapping).

For a homogeneous half-space, the ABFM result is an apparent conductivity equal to the half-space conductivity because the integral of the sensitivity function over  $z$  is unity. For a layered model with  $L$  layers having conductivities  $\sigma_j$  and depths to layer boundaries  $z_j$ , for  $j = 1, \dots, L$ ,  $z_1 = 0$  and for a discrete set of times  $t_i$ , equation (2) becomes

$$\sigma_a(t_i) = \sum_{j=1}^L \sigma_j \cdot F_{ij}, \quad (4)$$

where

$$F_{ij} = \int_{z_j}^{z_{j+1}} f(z, t_i, \sigma_a(t_i)) dz \\ = F(z_{j+1}, t_i, \sigma_a(t_i)) - F(z_j, t_i, \sigma_a(t_i)) \quad (5)$$

and  $F$  is the integrated sensitivity function (Figure 1b)

$$F(z, t, \sigma_a(t)) = \begin{cases} \frac{z}{d} \left( 2 - \frac{z}{d} \right) & \text{for } z \leq d \\ 1 & \text{for } z > d \end{cases} \quad (6)$$

ABFM is not explicitly defined because the apparent conductivity we wish to calculate enters in the coefficients  $F_{ij}$  required for the calculation. The mapping must therefore be realized iteratively. Many different methods exist to realize the iterative procedure, e.g., Newton iteration, but in this paper a fixed-point iteration procedure is implemented. This method has proven to be fast and robust. The mapping is initialized with an apparent conductivity equal to the average of the layer conductivities. With this starting value the apparent conductivity

is calculated according to equation (4), and with this improved estimate of the apparent conductivity the process is repeated until convergence. For high conductivity contrasts this procedure has been seen to bifurcate between two solutions. But if the apparent conductivity is only partly updated with the fraction  $\alpha$  of the new estimate according to the formula

$$\sigma_a^{k+1} \mapsto \alpha \sigma_a^{k+1} + (1 - \alpha) \sigma_a^k, \quad 0 < \alpha < 1, \quad (7)$$

the procedure becomes stable. A value of  $\alpha = 0.6$  has proven adequate; but to ensure a safety margin, a value of  $\alpha = 0.4$  was implemented. For  $\alpha = 0.4$ , the forward mapping converges typically in 5 to 10 iterations.

In Figure 2 the results of ABFM are compared with the exact all-time apparent conductivity based on the step response for a central-loop configuration with a loop area of 4 m<sup>2</sup>. A small loop has been chosen to simulate the response of coincident vertical magnetic dipole transmitter and receiver. For the central-loop configuration the all-time apparent conductivity is defined. The comparison is made for six models: two two-layer models and four three-layer models. Both models and model curves are displayed in Figure 2.

Comparisons have been made for values of the scaling parameter  $c$  in the interval from 2.62 to 3.04 in steps of 0.02. The choice that gave the smallest squared difference between the exact and the approximate apparent conductivity summed over the six models, was  $c = 2.8$ . Though this value is not optimal for all models, the choice is robust and close to optimal for most models.

As can be seen from Figure 2 the approximate apparent conductivity is generally a good approximation to the true apparent conductivity, especially for conductive layers. It is desirable for an approximate forward mapping that the approximation be good where well-resolved features of the model are expressed in the model response, whereas a poorer approximation can be tolerated for the parts of the model response that correspond to poorly determined parameters. The two-layer model with increasing conductivity with depth is very well modeled as expected because this model is the best resolved by transient EM data. The two-layer model with decreasing conductivity with depth is not as well modeled, as the one with increasing conductivity, but the poor conductor at depth is also not well resolved by transient EM data. The three-layer model with conductivity increasing steadily with depth is well modeled, as should be expected. For the three-layer model with a conductive layer between more resistive layers, the first part of the curve where conductivity is increasing is better modeled than the decreasing branch. For the three-layer model with a resistive layer between more conductive layers, the first part of the curve where conductivity is decreasing is modeled less well than the ascending branch. The three-layer model with conductivity decreasing steadily with depth shows, not surprisingly, the worst fit between the true and the modeled apparent conductivity.

ABFM produces an apparent conductivity that is a good approximation to the all-time apparent conductivity based on the step response of the central-loop configuration with a small loop.

According to the definition of ABFM,  $\sigma_a(t) \rightarrow \sigma_1$  for  $t \rightarrow 0$ . From Figure 2 we see that  $\sigma_a(t)$  approaches the conductivity of the bottom layer for  $t \rightarrow \infty$ . This is a result of optimizing

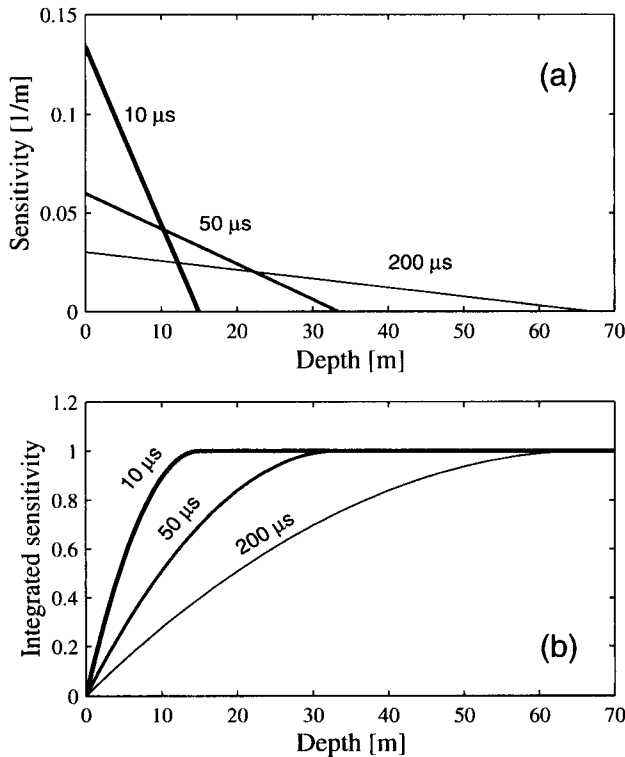


FIG. 1. (a) The sensitivity function as a function of depth for a half-space resistivity of 10 ohm-m and delay times of 10, 50, and 200 μs. (b) The corresponding integrated sensitivity functions.

the parameter  $c$ , entering in the scaled diffusion depth in equation (3). The deviation of ABFM apparent conductivity from the exact all-time apparent conductivity is most pronounced where the apparent conductivity changes rapidly, especially when it decreases. Thus, the higher the contrasts of the conductivity model, the larger the modeling error of the ABFM algorithm.

### The complete ABFM procedure

The complete ABFM procedure can be realized in this manner:

- 1) Calculate the apparent conductivity using ABFM.
- 2) For each delay time, calculate the step response as the response of a half-space with a conductivity equal to the apparent conductivity:  $H^{step}(t) = H_{half-space}^{step}(t, \sigma_a(t))$ .
- 3) From the step response, calculate the measured response by convolving with the time derivative of the current waveform.

Despite the fact that only a limited set of models and only the central-loop configuration have been studied, let us assume that ABFM with this value of  $c$  can be used for all configurations. To test the validity of this strong assumption, we compare the nonlinear responses for a number of different configurations, waveforms, and field components with the responses calculated using the complete ABFM procedure.

The results are seen in Figure 3. The full nonlinear responses have been calculated with the SELMA program (Christensen and Auken, 1992), and there are four configurations.

The first is a central-loop configuration with a transmitter loop of  $40 \times 40 \text{ m}^2$ , often used with the PROTEM 47 system from Geonics Ltd. The turn-off time is  $2.5 \mu\text{s}$ , the turn-on time is  $123 \mu\text{s}$ , and the repetition frequency is 25 Hz. A first-order filter with a cutoff frequency of 240 kHz is included in the system response. The  $z$ -component of  $dB/dt$  is modeled.

The second is an offset-loop configuration with a transmitter loop of  $40 \times 40 \text{ m}^2$  and a receiver coil 80 m from the loop center. The transmitter waveform is the same as in case 1. The  $z$ -component of  $dB/dt$  is modeled.

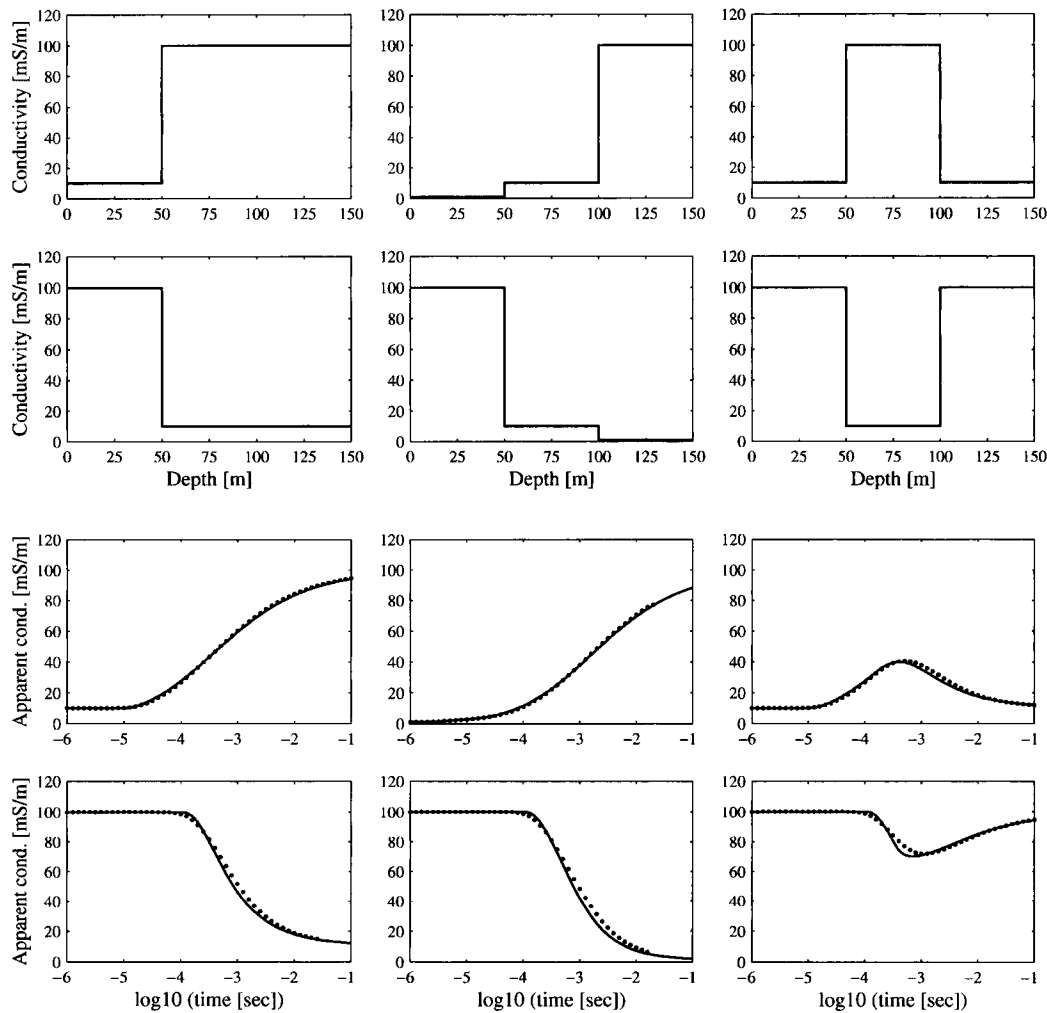


FIG. 2. Comparisons between the generic apparent conductivity and the nonlinear apparent conductivity of a central-loop configuration with a  $4\text{-m}^2$  transmitter for two two-layer models and four three-layer models. The models are seen in the top two rows of the plot. The conductivities of the models are 1, 10, and 100 mS/m, and layer boundaries are at 50 and 100 m. In the lower two rows the corresponding apparent conductivity curves are plotted. The dotted lines are the nonlinear all-time apparent conductivities; the full drawn curves are the ABFM apparent conductivities.

The third configuration is the Tempest airborne system from Fugro Ltd. with a 225-m<sup>2</sup> transmitter loop 120 m above the ground and a receiver 70 m above the ground, trailing 100 m behind the transmitter. The turn-off and turn-on times are 32  $\mu$ s, and the repetition frequency is 25 Hz. A first-order filter with a cutoff frequency of 37.5 kHz is included in the system response. The z-component of  $dB/dt$  is modeled.

The fourth configuration is the Geotem airborne system from Fugro Ltd. with a 225-m<sup>2</sup> transmitter loop 120 m above the ground and a receiver 70 m above the ground, trailing 125 m

behind the transmitter. The waveform is a half-sine of 2 ms duration, and the repetition frequency is 75 Hz. No filtering is modeled for the system response. The x-component of  $dB/dt$  is modeled.

The responses are calculated for two of the models from Figure 2: the two-layer model with a conductive basement and the three-layer model with a conductive layer between more resistive layers. ABFM produces responses very similar to the nonlinear responses for the central loop and the offset configuration over a wide time interval. For the offset configuration

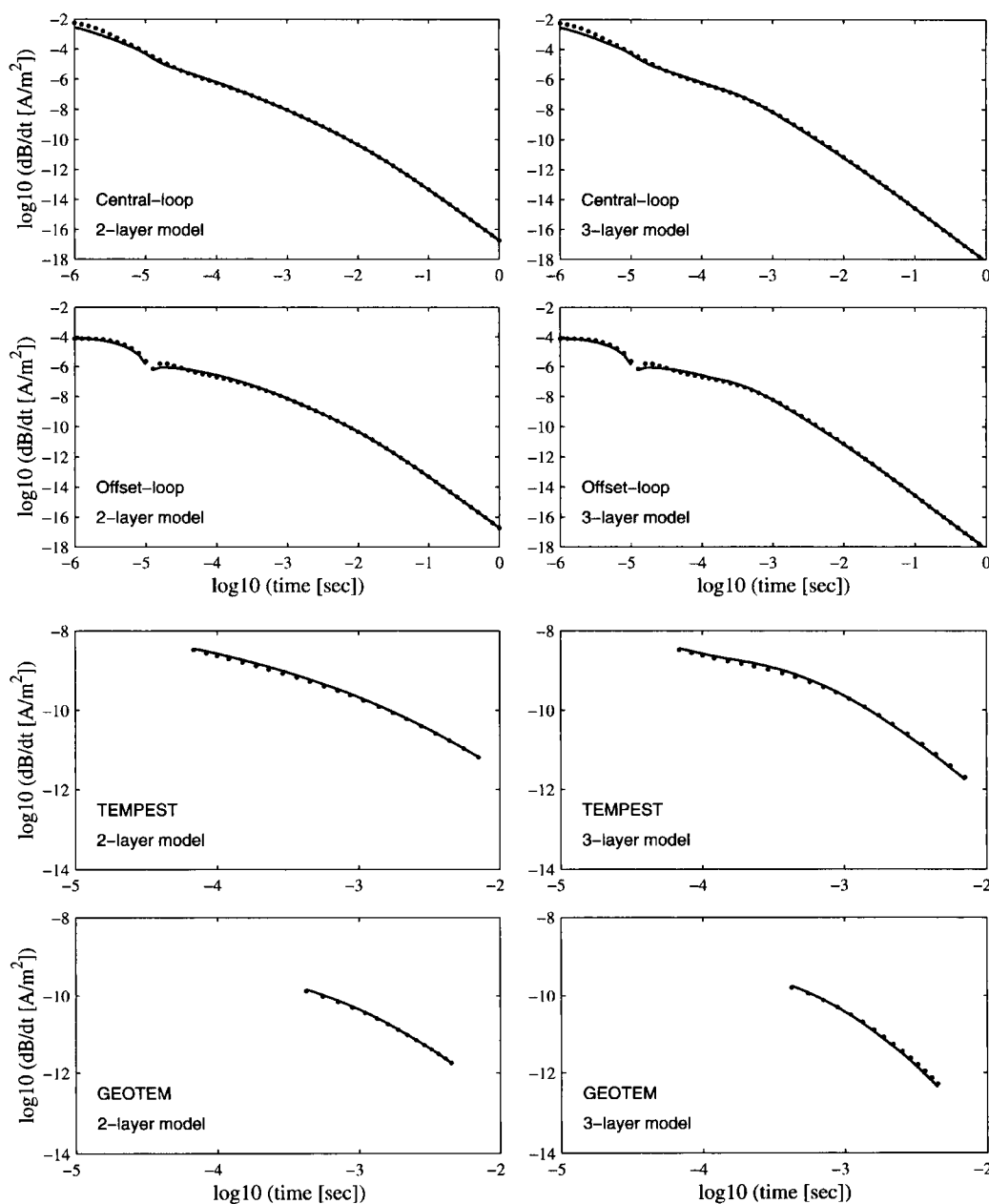


FIG. 3. Comparison between the true nonlinear responses (dotted) and the ABFM responses (solid) of four different transient EM configurations. In the left column the model is the two-layer model of Figure 2 with a conductive basement; in the right column the model is the three-layer model of Figure 2 with a conductive middle layer. From top to bottom: a central-loop configuration with a  $40 \times 40$  m<sup>2</sup> square transmitter loop; an offset-loop configuration with a  $40 \times 40$  m<sup>2</sup> square transmitter loop and a receiver offset of 80 m (the first part of the curves has negative sign); the Tempest airborne system; and the in-line horizontal component of the Geotem airborne system.

the sign shift is reproduced properly. For the airborne configurations the ABFM and nonlinear responses are almost identical. It is a pleasant surprise that ABFM initially developed for the vertical field of a small central-loop configuration also produces good results for the horizontal component of an airborne dipole–dipole configuration. The ability to model horizontal components has been verified also for ground-based systems.

**INVERSION**

Having established the complete ABFM procedure as consisting of a generic, configuration-independent forward mapping from layer conductivity to apparent conductivity followed by a configuration-dependent half-space response, the inversion using ABFM is straightforward. The separation of the problem into a generic part and a configuration-dependent part can be retained in the expressions for the derivatives. Because a measured response can be expressed in terms of the step response, the derivatives of a measured responses can be reduced to finding the derivatives of the step response.

For the step response the derivative with respect to layer conductivity is

$$\begin{aligned} \frac{\partial}{\partial \sigma_j} H_i^{step} &= \frac{\partial}{\partial \sigma_j} H_{half-space}^{step}(t_i, \sigma_a(t_i)) \\ &= \frac{\partial}{\partial \sigma_a} H_{half-space}^{step}(t_i, \sigma_a(t_i)) \times \frac{\partial \sigma_a(t_i)}{\partial \sigma_j}. \end{aligned} \quad (8)$$

The first term of the expression is configuration dependent and is the derivative of the response of a half-space with conductivity  $\sigma_a(t_i)$  with respect to its conductivity. The second part is configuration independent and is the derivative of the apparent conductivity with respect to the layer conductivity. According to equation (4),  $\partial \sigma_a(t_i)/\partial \sigma_j = F_{ij}$ .

Several avenues are open for calculating  $\partial H_{half-space}^{step}(t_i, \sigma_a(t_i))/\partial \sigma_a$ . The first approach is general and implies a calculation of a series of half-space responses for different conductivities followed by numerical differentiation. It is simple and sufficiently accurate, and the half-space responses need only be calculated once for a given configuration. For certain configurations, such as central-loop and dipole–dipole configurations on the surface, the half-space response depends on conductivity and time only through the parameter combination  $t/\sigma$ , leading to  $\partial H(t/\sigma)/\partial \sigma = (t/\sigma) \cdot \partial H(t/\sigma)/\partial t$ . In the late-time stage of transient diffusion, this relation also holds true for other configurations, e.g., those used by airborne systems. Therefore, if this approximation can also be accepted for early times, only one half-space response has to be calculated and differentiated with respect to time.

Derivatives with respect to layer thicknesses can be found in the same way as for conductivities. For the step response the derivative with respect to layer thickness  $h_j$  is

$$\begin{aligned} \frac{\partial}{\partial h_j} H_i^{step} &= \frac{\partial}{\partial h_j} H_{half-space}^{step}(t_i, \sigma_a(t_i)) \\ &= \frac{\partial}{\partial \sigma_a} H_{half-space}^{step}(t_i, \sigma_a(t_i)) \times \frac{\partial \sigma_a(t_i)}{\partial h_j}. \end{aligned} \quad (9)$$

Again, the first term of the expression is configuration dependent and is the derivative of the response of a half-

space with conductivity  $\sigma_a(t_i)$  with respect to its conductivity. The second part is configuration independent and is the derivative of the apparent conductivity with respect to layer thickness. According to equations (4) and (5), we have

$$\begin{aligned} \frac{\partial \sigma_a(t_i)}{\partial z_k} &= \frac{\partial}{\partial z_k} \sum_{j=1}^L \sigma_j \int_{z_j}^{z_{j+1}} f(z, t_i, \sigma_a(t_i)) dz \\ &= (\sigma_{k-1} - \sigma_k) f(z_k, t_i, \sigma_a(t_i)), \end{aligned} \quad (10)$$

whereby the derivative with respect to layer thickness  $h_k = (z_{k+1} - z_k)$  is given by

$$\frac{\partial \sigma_a(t_i)}{\partial h_k} = \sum_{j=k}^{L-1} (\sigma_j - \sigma_{j+1}) f(z_{j+1}, t_i, \sigma_a(t_i)). \quad (11)$$

**ONE-PASS IMAGING PROCEDURE**

For configurations for which it is possible to calculate the step response and the all-time apparent conductivity from the step response, it is possible to use equation (4) as a one-pass inverse. Adopting a multiple-layer model with fixed-layer boundaries and inverting only for the layer conductivities, an inverse model can be found by solving the linear set of equations of equation (4). The elements of the matrix in equation (4),  $F_{ij}$ , which depend on the apparent conductivity, can be found directly because the apparent conductivity is known from the data. Because the inversion scheme is approximate in nature, the errors introduced in  $F_{ij}$  from errors in the data can be accepted. Thus, the one-pass inverse retains the adaptive character without the need for an iterative calculation as is the case for ABFM.

This one-pass imaging approach is used by Christensen (1995) for central-loop sounding data. The step response was found from the measured response by expressing the step response as a sum of coefficients times a series of basis functions and solving a linear set of equations for the coefficients. Once the step response is found, the all-time apparent conductivity can be determined uniquely for the central-loop configuration. In the paper by Christensen (1997), the one-pass inverse approach is used in a 2-D imaging algorithm.

In Figure 4 the performance of the one-pass 1-D inversion is demonstrated. The inversion is done by solving equation (4). The inversion is realized as a constrained least-squares inversion through the formula

$$\sigma = (\mathbf{F}^T \mathbf{C}_e^{-1} \mathbf{F} + \mathbf{E} + \mathbf{S})^{-1} \mathbf{F}^T \mathbf{C}_e^{-1} \sigma_a, \quad (12)$$

where  $\mathbf{F}$  is the matrix containing the elements  $F_{ij}$ ,  $\sigma$  is the layer conductivities,  $\sigma_a$  is the apparent conductivity data,  $\mathbf{C}_e^{-1}$  is the inverse of the data error covariance matrix,  $\mathbf{E}$  is the roughness matrix constraining the flatness of the model, and  $\mathbf{S}$  is a diagonal matrix constraining the smallness of the model (Menke, 1989). The data error is assumed to be Gaussian distributed, and the matrices are given by

$$\mathbf{C}_e^{-1} = \left( \frac{1}{\Delta \sigma_a} \right)^2 \mathbf{I}, \quad \mathbf{S} = \left( \frac{1}{\Delta_s} \right)^2 \mathbf{I}, \quad \mathbf{E} = \left( \frac{1}{\Delta_r} \right)^2 \mathbf{R}, \quad (13)$$

where  $\mathbf{R}$  is the roughness matrix.

$$\mathbf{R} = \begin{bmatrix} 1 & -1 & 0 & \cdot & 0 & 0 & 0 \\ -1 & 2 & -1 & \cdot & 0 & 0 & 0 \\ 0 & -1 & 2 & \cdot & 0 & 0 & 0 \\ \cdot & \cdot & \cdot & \cdot & \cdot & \cdot & \cdot \\ 0 & 0 & 0 & \cdot & -1 & 2 & -1 \\ 0 & 0 & 0 & \cdot & 0 & -1 & 1 \end{bmatrix} \quad (14)$$

In the inversions in Figure 4, the constraints are rather weak;  $\Delta\sigma_a$  was set to 1 mS/m and  $\Delta_r = \Delta_r = 50 \cdot \Delta\sigma_a$ . No noise was added to the data before inversion.

The models obtained through the one-pass inverse are good approximations to the true models, taking the abilities of the transient method into account: good conductors are well determined and poor conductors are not. Figure 4 compares the true apparent conductivity data and the full nonlinear forward responses of the inverted models. Good consistency is observed, and the deviation is generally  $<5\%$ . Hence, the imaged models fit the data within what is normally considered to be the noise level of the data.

#### EXAMPLES OF INVERSION WITH ABFM IMAGING

ABFM imaging can easily be included in any 1-D inversion program normally used to interpret transient EM data. The

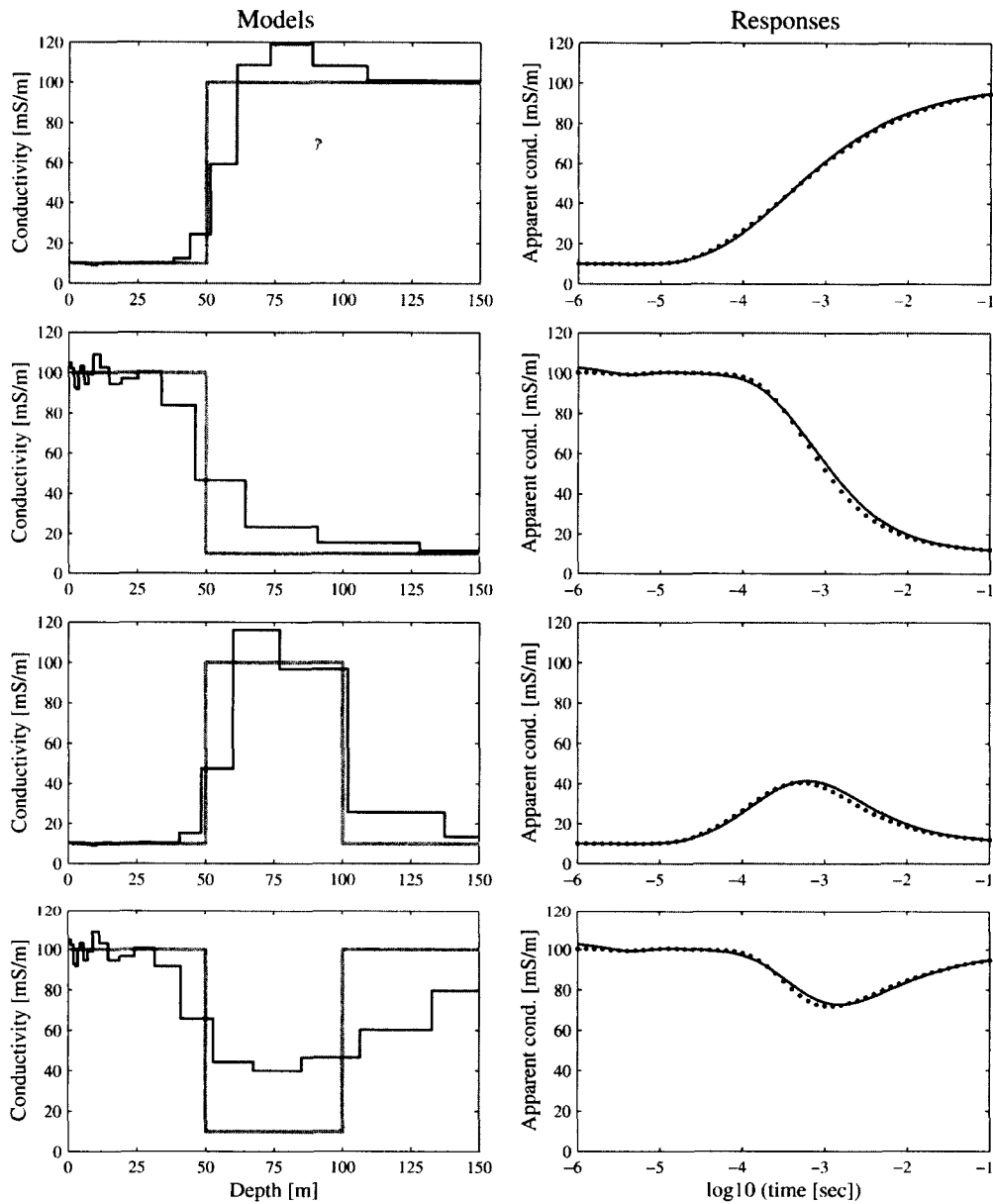


FIG. 4. (Left column) The models obtained from a one-pass inverse of central-loop data using the expression in equation (4), shown in black, compared with the true models, shown in gray. The models are identical to four of the models of Figure 2. (Right column) Comparison between the true all-time apparent resistivity data (dotted) and the full nonlinear response (solid) calculated for the inverted models in the left column.

efficacy of the imaging algorithm is demonstrated by comparing the imaging results with the results of full nonlinear inversion for three case histories, as seen in Figure 5.

The first example is from Krannestrup in eastern Jutland, Denmark, where Quaternary deposits of till and sand are underlain by Danien Limestone. Central-loop transient EM soundings with a  $40 \times 40 \text{ m}^2$  transmitter loop were performed every 20 m on a north–south profile using Geonics Protem 47 equipment. A well-conducting clay is present in the southern parts of the profile but thins out toward the north where it vanishes. Unfortunately, part of the profile had to be discarded because of coupling to a buried cable. Interpretations were

done with a 12-layer model with layer thicknesses increasing with depth as a hyperbolic sine function. The layer boundaries are fixed, and only conductivities are free parameters in the inversion. Inversion was initialized with a 30 ohm-m homogeneous half-space. Regularization is implemented by claiming identity between conductivities of neighboring layers with a relative uncertainty of 0.15. The optimization problem is solved with an  $L_1$ -norm to produce more blocky models (Farquharson and Oldenburg, 1998), as conductivity changes are expected to be abrupt. There is almost no difference between the model sections obtained with the ABFM imaging and a full nonlinear inversion. Both model sections reveal a covering layer of

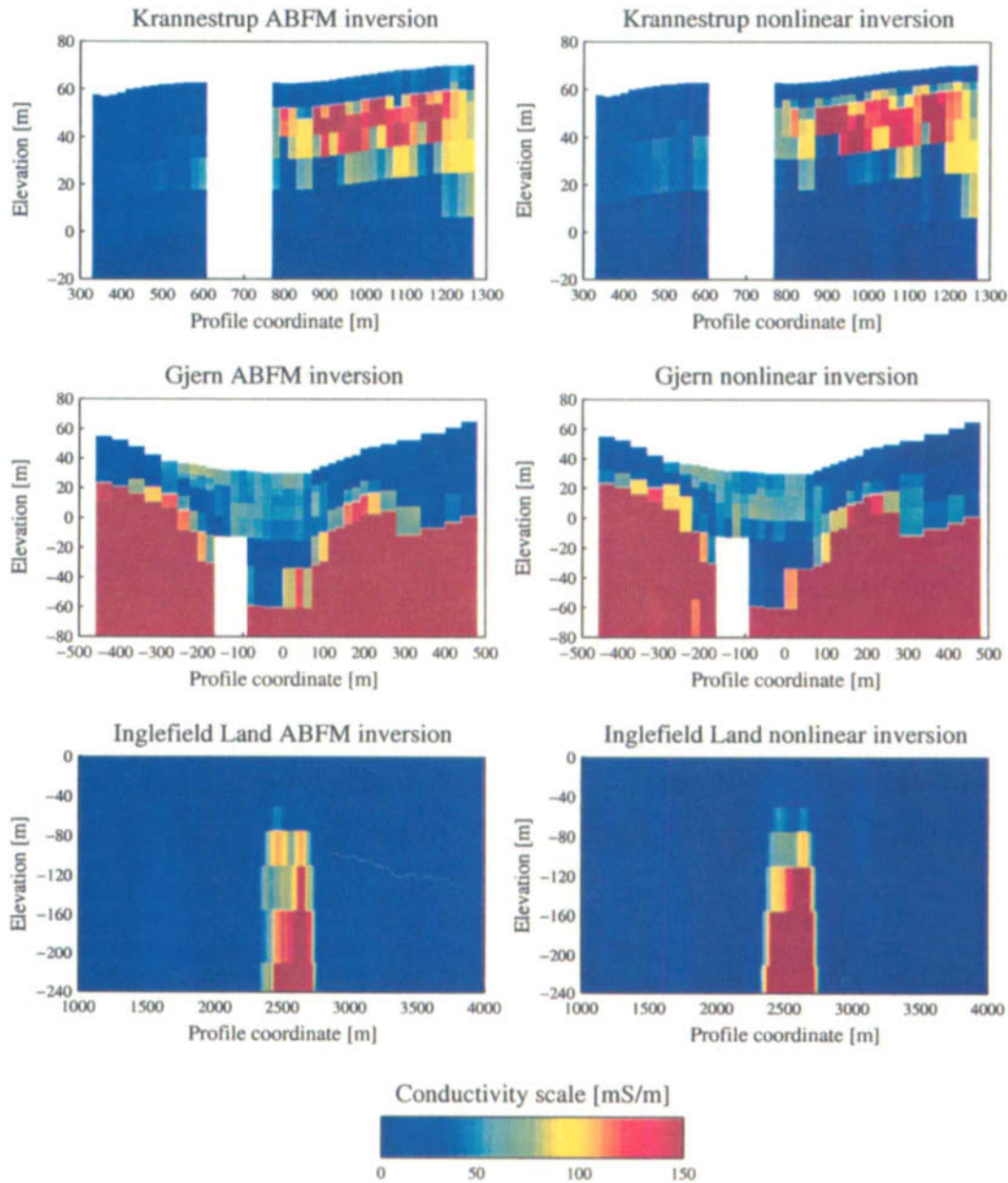


FIG. 5. Comparison between ABFM imaging (left column) and full nonlinear inversion (right column) of field data. (Top row) Central-loop data on a north (left)–south (right) profile from Krannestrup, Jutland, Denmark. (Middle row) Central-loop data from Gjern, Jutland, Denmark. (Bottom row) Airborne  $x$ -component data measured with the GEOTEM system from Inglefield Land, Greenland.

fairly high resistivity underlain by the wedge of well-conducting clay. Below the clay is the high-resistivity, freshwater-saturated Danien Limestone.

The next example is from Gjern in central Jutland, Denmark. A profile of central-loop soundings with a  $40 \times 40 \text{ m}^2$  transmitter loop was run west to east with Geonics Protem 47 equipment across the Gjern River. Distance between soundings was 20 m in the central parts of the profile and 40 m at the profile ends. The transient EM survey was designed to investigate why the river runs linearly over an unusually long stretch. The hypothesis was that the linearity was the result of recent, ongoing tectonic movements. Under the Quaternary sequence of tills and sand lies a Tertiary clay. Any tectonic movements that may have taken place should be detectable in the relief of the Tertiary clay. The clay is a good conductor, and the transient EM method is thus ideal for mapping any possible depression in the clay. Once more, however, the profile was affected by the presence of a power line and three of the soundings were disturbed by coupling phenomena, except for a few early time channels. For this reason the resulting models were truncated at 45 m depth because they contained no information on the deeper parts. Inversion was done with the same 12-layer model as in the previous example, and the initial model had a resistivity of 30 ohm-m down to 63 m and 5 ohm-m below. The inversion results clearly show the presence of a narrow valley in the Tertiary clay and support the assumption of the river valley being the result of tectonic events. The inversion results using ABFM imaging and the full nonlinear inversion display similar features but in this example there is slightly more difference than in the Krannestrup example—especially in the central parts of the valley. This is attributed to the fact that the geological model has 2-D features that are not well modeled with 1-D models.

The third example is a model section of concatenated 1-D interpretation of data of the horizontal in-line component of the Geotem system from Inglefield Land, Greenland (Stemp and Thorning, 1995a,b). The geology of the area is not one dimensional; nevertheless, 1-D concatenated interpretations will point to places where good conductors are present and also enable an estimate of depth of burial. The conductive anomaly seen in the plot is interpreted to be a steeply dipping, plate-shaped conductor. In this case there is more difference between the imaged models and the models obtained from nonlinear inversion, especially in the apparent depth to the conductor, than seen in the previous examples. This imaging algorithm does not perform well in a parametric inversion with few layers, where both conductivities and layer thicknesses are updated in the inversion process. The imaging algorithm can give rise to interpreted models that differ from the ones returned by a nonlinear inversion. Even the depth to a good conductor normally determined well in a transient EM sounding is determined incorrectly by the imaging algorithm. In the case of models with fixed layer boundaries, the imaging algorithm performs well because transient EM data are more linear in conductivity than in layer thickness.

## DISCUSSION

The ABFM imaging has a series of advantages over other popular imaging algorithms. Most imaging algorithms are based on the ideal step response of the measurement system

and require that the step response be estimated from the measured data. However, the estimation of the step response is a deconvolution process and is inherently unstable. Using inversion to recover the step response (Christensen, 1995; Stolz and Macnae, 1998) typically requires some ad hoc regularization. Contrary to this, the ABFM imaging algorithm used with multiple-layer models only involves stable forward computations and convolutions. The regularization used by the ABFM algorithm has a direct reference to the assumed statistical properties of the model because it involves only a formulation of a model covariance function for the subsurface conductivity or, equivalently, constraints on the smallness and/or flatness of the model.

Some imaging procedures require that the all-time apparent conductivity be determined from the step response (Christensen, 1995) or, equivalently, a reference arrival time (Polzer, 1985). This is possible for certain measurement configurations (e.g., central loop). But if the step response is not a monotonic function of conductivity, as for a dipole-dipole configuration, this problem does not have a unique solution and such imaging becomes impossible. ABFM imaging does not require these transformations. The apparent conductivity is always forward calculated and then substituted into a half-space response.

The inversion procedure using ABFM imaging is iterative. Therefore, nothing is lost by working with the logarithm of the conductivity and thereby avoiding negative values. ABFM imaging also accommodates the use of both an  $L_1$  and an  $L_2$  norm in the inversion. The  $L_1$  norm produces blocky models (Farquharson and Oldenburg, 1998) and is thus useful when the conductivity structure is expected to have abrupt changes.

As pointed out by Effersø et al. (1999), it is generally necessary to incorporate the fact that transient EM instruments have a limited frequency range by modeling the band-limited behavior in the forward modeling and the calculation of the derivatives. ABFM imaging can easily be incorporated into modeling the band-limited behavior by calculating band-limited half-space responses.

The possibility of having a near-real-time overview of the subsurface conductivity structure is important in many cases, especially for large data sets such as airborne surveys. The imaged models can furthermore serve as good starting models for a refined interpretation involving full nonlinear calculations, saving considerable effort.

The price paid for the generality of ABFM imaging is that it becomes iterative instead of one pass. However, this is not a real limitation. ABFM imaging is extremely fast because the calculations of the sensitivity function and its integral involve very few arithmetic operations on account of their simplicity. ABFM imaging has been used for the inverse modeling of Geotem  $x$ -component data from Inglefield Land, Greenland (Poulsen et al., 1999a,b), where 17 000 line kilometers of data with a 10-m sample spacing were inverted. The sounding data sets were comprised of 12 data points, and the inversion was done with a 9-layer model. On a 200-MHz Pentium II computer, processing could be done at a speed of  $\approx 50$  soundings per second. The results were practically indistinguishable from nonlinear inversions. Two-thirds of the 1.7 million soundings had a data quality that did not warrant a quantitative inversion. The remaining 500 000–600 000 soundings were inverted in 4 hours.

Christensen (1997) shows that the one-pass approach also gives satisfactory results for 2-D problems. It is expected that the ABFM inversion developed in this paper for the 1-D case will also be valid for the 2-D case and thereby give generality in terms of configuration and waveform to 2-D transient EM inversion problems.

### CONCLUSION

An imaging algorithm for 1-D inversion of transient EM data has been presented based on an approximate forward mapping using the adaptive Born approximation. ABFM is given implicitly and is realized through an iterative scheme. ABFM imaging is generally applicable for all waveforms and all geometrical configurations, land-based and airborne, for which the half-space response can be calculated. It is stable because it does not involve deconvolution operations or nonunique transformations.

The ABFM imaging method involves only simple arithmetic operations and is easy to program. Computation is rapid and allows typically 10–100 soundings to be inverted per second. It is ideally suited for inversion of large data sets, such as airborne surveys or land-based continuous methods, to provide a fast overview of the subsurface conductivity. ABFM-imaged models serve as good starting models for a nonlinear refinement of the interpretation. ABFM imaging offers on-line interpretation in the field for quality control and decisions about survey strategy.

### ACKNOWLEDGMENTS

Thanks to Louise Pellerin for an informal review and to Ned Stolz, an anonymous reviewer, and Associate Editor David Boerner for constructive comments. Mads W. Toft walked on water to collect the Gjærn data set (in the winter), and the Geological Survey of Denmark and Greenland (GEUS) kindly provided the Inglefield Land data.

### REFERENCES

- Buselli, G., Barber, C., Davis, G. B., and Salama, R. B., 1990, Detection of groundwater contamination near waste disposal sites with transient electromagnetic and electrical methods, *in* Ward, S. H., Ed., *Geotechnical and environmental geophysics 2, Environmental and groundwater: Soc. Expl. Geophys. Investigations in Geophysics 5*, 27–39.
- Christensen, N. B., 1995, Imaging of central-loop transient electromagnetic soundings: *J. Environ. and Eng. Geophys.*, **0**, No. 1, 53–66.
- 1997, Electromagnetic subsurface imaging—A case for an adaptive Born approximation: *Surveys in Geophys.*, **18**, 477–510.
- Christensen, N. B., and Auken, E., 1992, Simultaneous electromagnetic layered model analysis, *in* Jacobsen, B. H., Ed., *Proceedings of the Interdisciplinary Inversion Workshop 1, Aarhus 1992: GeoSkrifter*, **41**, 49–56.
- Christensen, N. B., and Sørensen, K. I., 1998, Surface and borehole electric and electromagnetic methods for hydrogeophysical investigations: *Eur. J. Environ. Eng. Geophys.*, **3**, No. 1, 75–90.
- Eaton, P. A., and Hohmann, G. W., 1989, A rapid inversion technique for transient electromagnetic soundings: *Phys. Earth Plan. Int.*, **53**, 384–404.
- Effersø, F., Auken, E., and Sørensen, K. I., 1999, Inversion of band-limited transient EM responses: *Geophys. Prosp.*, **47**, 551–564.
- Farquharson, C., and Oldenburg, D. W., 1998, Nonlinear inversion using general measures of data misfit and model structure: *Geophys. J. Internat.*, **34**, 213–227.
- Fittermann, D. V., and Stewart, M. T., 1986, Transient electromagnetic sounding for groundwater: *Geophysics*, **51**, 995–1005.
- Gomez-Treviño, E., 1987, Nonlinear integral equations for electromagnetic inverse problems: *Geophysics*, **52**, 1297–1302.
- Hoekstra, P., and Blohm, M. W., 1990, Case histories of time-domain electromagnetic soundings in environmental geophysics, *in* Ward, S. H., Ed., *Geotechnical and environmental geophysics 2, Environmental and groundwater: Soc. Expl. Geophys. Investigations in Geophysics 5*, 1–16.
- Macnae, J. C., and Lamontagne, Y., 1987, Imaging quasi-layered conductive structures by simple processing of transient electromagnetic data: *Geophysics*, **52**, 545–554.
- Macnae, J. C., Smith, R., Polzer, B. D., Lamontagne, Y., and Klinkert, P. S., 1991, Conductivity-depth imaging of airborne electromagnetic step-response data: *Geophysics*, **56**, 102–114.
- Menke, W., 1989, *Geophysical data analysis: Discrete inverse theory: Academic Press Inc.*
- Nekut, A. G., 1987, Direct inversion of time-domain electromagnetic data: *Geophysics*, **52**, 1431–1435.
- Polzer, B. D., 1985, The interpretation of inductive transient magnetic sounding data: *Res. in Appl. Geophys.*, **36**, University of Toronto.
- Poulsen, L. H., Rasmussen, T. M., and Christensen, N. B., 1999a, Interpretation of airborne measurements over Inglefield Land, Northwest Greenland: 61st Meeting and Technical Exhibition, *Eur. Assn. Geosci. Eng., Proceedings*, P030.
- 1999b, Interpretation strategies for airborne measurements: The Inglefield Land survey: *Advances in Expl. Geoelectromag. Eur. Assn. Geosci. Eng., Proceedings*.
- Smith, R. S., Edwards, R. N., and Buselli, G., 1994, An automatic technique for presentation of coincident-loop, impulse-response, transient, electromagnetic data: *Geophysics*, **59**, 1542–1550.
- Sørensen, K. I., 1997, The pulled array transient electromagnetic method: 3rd meeting, Environmental and Engineering Geophysical Society—European Section, *Proceedings*, 135–138.
- Sørensen, K. I., Auken, E., and Thomsen, P., 2000, TDEM in groundwater mapping—A continuous approach: *Symposium on Appl. of Geophys. to Eng. and Environ. Problems, Proceedings*, 485–491.
- Sørensen, K. I., Effersø, F., and Christensen, A. J., 1995, Pulled array transient electromagnetic method (PATEM): *Symposium on Appl. of Geophys. to Eng. and Environ. Problems, Proceedings*, 899–904.
- Spies, B. R., and Eggers, D. E., 1986, The use and misuse of apparent resistivity in electromagnetic methods: *Geophysics*, **51**, 1462–1471.
- Stolz, R. W., and Thorning, L., 1995a, Airborne electromagnetic and magnetic survey of Inglefield Land, northwest Greenland: *Geological Survey of Denmark and Greenland*, **95/1**.
- 1995b, A new airborne electromagnetic and magnetic survey of Inglefield Land, northwest Greenland: *Project AEM Greenland 1994–1998: Geol. Surv. of Denmark and Greenland, Report of Activities* **165**, 64–68.
- Stolz, E., and Macnae, J., 1997, Fast approximate inversion of transient EM data: *Expl. Geophys.*, **28**, No. 3, 317–322.
- 1998, Evaluating EM waveforms by singular-value decomposition of exponential basis functions: *Geophysics*, **63**, 64–74. (Errata in *Geophysics*, **64**, 310).